RESEARCH ARTICLE

Ultrasound-guided breast biopsy using an adapted automated cone-based ultrasound scanner: a feasibility study

Anton V. Nikolaev[1] | **Leon de Jong**[1] | **Patrik Zamecnik**[1] | **Vincent Groenhuis**[2] | **Françoise J. Siepel**[2] | **Stefano Stramigioli**[2] | **Hendrik H.G. Hansen**[1] | **Chris L. de Korte**[1,3]

[1]Medical Ultrasound Imaging Center (MUSIC), Department of Medical Imaging/Radiology, Radboud University Medical Center, Nijmegen, The Netherlands

[2]Robotics and Mechatronics, University of Twente, Enschede, The Netherlands

[3]Physics of Fluids Group, TechMed Center, University of Twente, Enschede, The Netherlands

Correspondence
Anton V. Nikolaev, Medical Ultrasound Imaging Center (MUSIC), Department of Medical Imaging/Radiology, Radboud University Medical Center, Nijmegen 6525 GA, The Netherlands.
Email: a.nikolaev@erasmusmc.nl

Abstract

Background: Among available breast biopsy techniques, ultrasound (US)-guided biopsy is preferable because it is relatively inexpensive and provides live imaging feedback. The availability of magnetic resonance imaging (MRI)-3D US image fusion would facilitate US-guided biopsy even for US occult lesions to reduce the need for expensive and time-consuming MRI-guided biopsy. In this paper, we propose a novel Automated Cone-based Breast Ultrasound Scanning and Biopsy System (ACBUS-BS) to scan and biopsy breasts of women in prone position. It is based on a previously developed system, called ACBUS, that facilitates MRI-3D US image fusion imaging of the breast employing a conical container filled with coupling medium.

Purpose: The purpose of this study was to introduce the ABCUS-BS system and demonstrate its feasibility for biopsy of US occult lesions.

Method: The biopsy procedure with the ACBUS-BS comprises four steps: target localization, positioning, preparation, and biopsy. The biopsy outcome can be impacted by 5 types of errors: due to lesion segmentation, MRI-3D US registration, navigation, lesion tracking during repositioning, and US inaccuracy (due to sound speed difference between the sample and the one used for image reconstruction).

For the quantification, we use a soft custom-made polyvinyl alcohol phantom (PVA) containing eight lesions (three US-occult and five US-visible lesions of 10 mm in diameter) and a commercial breast mimicking phantom with a median stiffness of 7.6 and 28 kPa, respectively. Errors of all types were quantified using the custom-made phantom. The error due to lesion tracking was also quantified with the commercial phantom.

Finally, the technology was validated by biopsying the custom-made phantom and comparing the size of the biopsied material to the original lesion size. The average size of the 10-mm-sized lesions in the biopsy specimen was 7.00 ± 0.92 mm (6.33 ± 1.16 mm for US occult lesions, and 7.40 ± 0.55 mm for US-visible lesions).

Results: For the PVA phantom, the errors due to registration, navigation, lesion tracking during repositioning, and US inaccuracy were 1.33, 0.30, 2.12, and 0.55 mm. The total error was 4.01 mm. For the commercial phantom, the error due to lesion tracking was estimated at 1.10 mm, and the total error was 4.11 mm. Given these results, the system is expected to successfully biopsy lesions larger

than 8.22 mm in diameter. Patient studies will have to be carried out to confirm this in vivo.

Conclusion: The ACBUS-BS facilitates US-guided biopsy of lesions detected in pre-MRI and therefore might offer a low-cost alternative to MRI-guided biopsy. We demonstrated the feasibility of the approach by successfully taking biopsies of five US-visible and three US-occult lesions embedded in a soft breast-shaped phantom.

KEYWORDS
breast biopsy, image fusion, ultrasound-guided biopsy

1 | INTRODUCTION

One out of seven women will get breast cancer, and in 11 countries of the world, it is even the most frequent cause of death.[1] Early and reliable diagnosis is of paramount importance for the timely treatment of breast cancer since early diagnosis reduces mortality and morbidity.[2] After mammography, ultrasound (US) imaging of a lesion with subsequent breast biopsy is a common clinical practice to determine whether the lesion is malignant or benign.[3] However, the sensitivity of US for the detection of lesions is limited to approximately 80%.[4] For high-risk populations and for patients with mammographically and US occult lesions, magnetic resonance imaging (MRI) is performed. MRI outperforms US and mammography in terms of sensitivity. However, MRI is an expensive and time-consuming modality.[5]

Among available breast biopsy techniques, an ultrasound-guided biopsy (UGB) is preferable. In comparison to MRI- or stereotactic-guided biopsies, UGB provides real-time guidance of the needle and is cost-effective, less invasive, and the entire biopsy procedure takes less time.[6,7] In clinical routine, UGB is performed with a patient in the supine position.[6]

However, there are two main limitations that impede the use of US for biopsy guidance. First, the outcome of the ultrasound-guided biopsy strongly depends on the operator, that is, radiologist,[6,8] which can lead to false-negative diagnosis.[6,8–10] One study reported a false-negative rate as high as 36%.[8] Second, UGB is possible only if the lesion is easily detectable with US.[7,11] Otherwise, MRI with subsequent MRI-guided biopsy might be performed.[12]

The availability of MRI-US image fusion would facilitate US-guided biopsy even for US occult lesions and simplify the work of radiologists by simplified lesion detection. A study by Piron and co-workers demonstrated the feasibility of successful MRI–US fusion-based breast biopsy.[13] They demonstrated that the fusion of MRI with 2D US improved the diagnostic accuracy of the biopsy process by 10% with a registration accuracy of 1.5 mm. Image fusion was not problematic since the breast was rigidly fixed at the same position during MRI and biopsy.[13] In this approach the MRI acquisitions, and UGB have to be performed immediately successively since the patient has to remain in the same position. Consequently, MRI scanning on one day and biopsy taking on another day is not allowed with this approach. Usually in clinic these two operations are not performed immediately successively because first the radiologist needs to judge the images on the presence of malignancy which requires time. Also, this approach requires the use of a detachable table which is not always part of a conventional MRI setup. However, probably the biggest disadvantage is that the MRI setup remains occupied for other patients while performing UGB.

In the current study, we introduce a novel breast biopsy approach that does not require fixation of the breast and therefore allows separation of MRI pretreatment scanning and US-based biopsy taking. We introduce an Automated Cone-based Breast Ultrasound Scanning and Biopsy System (ACBUS-BS). It is based on a previously developed ACBUS system that facilitates MRI-3D US image fusion imaging of the breast employing a conical container filled with a coupling medium.[14] Thus, the target lesion can be identified either with 3D US, which is routinely used as a second-look imaging modality or through MRI-3D US image fusion in case the lesion is US-occult. The ACBUS-BS provides the interventionist access to the breast surface before the needle intervention.

In this paper, we analyze the feasibility of the ACBUS-BS as a potential alternative to MRI-guided biopsy. Using a custom-made and a commercial breast-mimicking phantoms, we evaluate the metrics influencing the biopsy outcome. Finally, we evaluated the performance of the system by taking biopsies of the custom-made phantom.

2 | MATERIALS AND METHODS

2.1 | Breast phantoms

A breast phantom was created to quantitatively evaluate the tracking and registration accuracies, and biopsy

outcome for the designed system. For the phantom to be suitable it had to satisfy a number of requirements. First, it had to be MRI and US compatible. Second, it had to mimic the breast as close in terms of mechanical properties and geometry. Breast tissue stiffness, that is, Young's modulus values have been reported ranging from 0.5 to 25 kPa for adipose tissue and from 7.5 to 66 kPa for glandular tissue.[15] Next, the lesions should be of variable level of homogeneity and echogenicity, mimicking the in vivo cases as was reviewed by Gokhale et al. in.[16] Specifically, the phantom should contain isoechoic homogeneous and inhomogeneous inclusions that are in general challenging to find in the breast during conventional US-guided biopsy. The hyperechoic lesions can serve as validation markers for registration accuracy and mimic ultrasound visible lesions. Finally, the lesions should be stained with a color different from the background to quantify biopsy accuracy.

Taking into consideration the abovementioned requirements, it was decided to fabricate a custom polyvinyl alcohol (PVA) breast phantom with US-occult and high contrast lesions. The PVA material is widely used for tissue-mimicking phantoms and is MRI and US-compatible as was demonstrated by Surry et al.[17] The PVA phantom was developed to calculate the accuracy metrics and to evaluate a biopsy performance of US-visible and US-occult lesions. To mimic the mechanical properties of a breast as close as possible, the phantom was made of a low concentration of PVA. The phantom included eight spherical stained inclusions of 10 mm nominal diameter mimicking lesions, which also serve as biopsy targets. There are three lesions that have low contrast with respect to the background to mimic isoechoic lesions, while the remaining five lesions have high contrast mimicking hyperechoic lesions and are also used to measure registration accuracy. Both inclusions and the background are homogeneous. The 3 low contrast lesions are located at depth less than 10 mm from the surface of the phantom.

The high and low contrast inclusions were fabricated first in separate batches. Polyvinyl Alcohol (10% by weight, PVA, Acros organics, Geel, Belgium) was dissolved in ethylene glycol (40% by volume) and distilled water (60% by volume) at 90°C. Next, 5% by weight of black ink was added to stain the inclusions. The resulting solution was stirred with a magnetically steered stirring rod at 500 rpm for 1.5 hours. Silica gel particles of 60–100 μm and <40 μm size for high and low contrast lesions respectively (1% by weight, Merck KGaA, Darmstadt, Germany) with Dotarem gadolinium (1.5 ml/l, Guerbet, Villepinte, France) were added 10 minutes before stopping stirring. Next, the resulting solutions were cooled down to 22°C, poured in spherical molds, and went through one freeze-thaw cycle. Finally, similar to our previous study,[14] the lesions were positioned in a breast-shaped mold using strings. The mold was designed to mimic the breast's shape and 3D printed with polylactide (PLA) material.
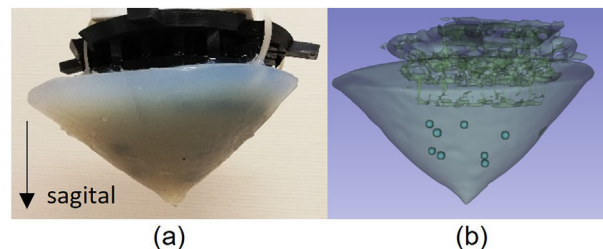

FIGURE 1 PVA breast phantom (a) overview and (b) rendered MRI with eight inclusions embedded. The black arrow indicates the sagittal direction.

The background material was fabricated by dissolving PVA (5% by weight) in the 40% ethylene glycol. 60% distilled water solution (89% by weight) at 90°C, while stirring with a magnetically steered stirring rod at 500 rpm for 1.5 h. The lower amount of PVA could lead to a poorly attached phantom to the holder. For acoustic scattering, silica particles (<40 μm size) were added to the solution 10 min before stopping stirring. Next, the resulting PVA solution was cooled down to 22°C, and poured into a mold. The 3D-printed PLA holder (Figure 1a) was submerged in the top layer of the PVA solution, and the resulting construction underwent one freeze-thaw cycle. Hence, the lesions underwent two freeze-thaw cycles, and the surrounding material only one. The manufactured phantom is shown in Figure 1.

In the fabricated PVA phantom, both lesions and the background have homogeneous structure and do not fully mimic a real breast. Therefore, we also incorporated a commercial CIRS M73 phantom (InMed, Seven Hills, USA). The CIRS phantom is routinely used for biopsy training and mimics the breast structure: skin, internal inhomogeneity, and internal lesions. For validation, we selected in the CIRS phantom a spherical lesion (∼5 mm in diameter) which also has a low contrast with its background.

For each type of selected lesions, we calculated the contrast to noise ratio (CNR)[18] with the formula below:

$$CNR = 20 log_{10} \frac{|\mu_l - \mu_b|}{\sqrt{0.5 \left(\sigma_l^2 + \sigma_b^2 \right)}}, \quad (1)$$

where μ_l, end μ_b are mean echo levels within the lesion and background areas, respectively, and σ_l and σ_b are the standard deviations of the echo levels within the lesion and the background, respectively.

The stiffnesses of the custom-made PVA and CIRS phantoms were measured with an Aixplorer Ultimate ultrasound system (Hologic Supersonic imagine, Aix-en-Provence, France) utilizing shear wave elastography mode. The stiffnesses were calculated for 7 ROI's randomly distributed within each phantom. The speed of sound of the PVA phantom was determined by
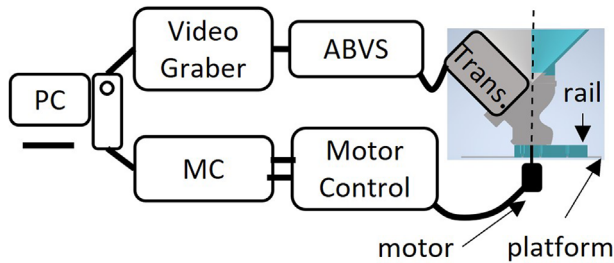
FIGURE 2 ACBUS-BS design overview. ABVS, Automated Breast Volumetric System; MC, Microcontroller; PC, Personal Computer (workstation).

measuring the thickness of the PVA block sample (9.2 mm thick) in B-mode US image. The block was cut from the phantom after the biopsy had been performed.

2.2 | System design

The design of the ACBUS-BS is schematically represented in Figure 2. We based the system on a Siemens ACUSON S2000 Automated Breast Volumetric Scanner (ABVS) platform (Siemens Ultrasound, Issaquah, WA, USA). A 14L5BV transducer (Siemens Medical Solutions, Mountain View, California, USA) of 152 mm length was detached from a Breast ABVS robotic arm (Siemens Medical Solutions, Mountain View, California, USA) and integrated into the wall of a 3D printed PLA cone-shaped container, which will be referred to as "cone" throughout the manuscript. The cone's assembly is presented in Figure 3. Cone parts were designed in a CAD system and printed using an Ultimaker 3D printer (Ultimaker, Utrecht, the Netherlands) with PLA material. The printer has a 0.4 mm nozzle size, which was taken into consideration while designing. The cone is inserted into the rail (Figure 3a—e), which facilitates its translation in the direction shown in Figure 3a. The half of the cone can be detached (Figure 3a,b) and replaced by the biopsy slit holder (Figure 3e—g). Next, the biopsy slit (Figure 3e—h) can be inserted into the slit holder as shown in Figure 3c and e. The biopsy slit was designed to keep the biopsy needle within the B-mode US image and is located in front of the US transducer array (Figure 3e). The slit can be translated as show in Figure 3c by moving it within the slit holder (Figure 3e). The slit gap width was designed to fit a 14 G biopsy needle and equal to its outer diameter of ∼2.133 mm. The slit was designed to have a length of 7 mm (Figure 3e) to prevent wobbling of the needle.

The rail is integrated on the top of the rotating platform (Figures 2 and 3a–d), actuated by a closed-loop stepper motor ARM69AC (Oriental Motor, Torrance, USA) with a discrete rotational step size of 0.36° and connected to the motor control unit (Figures 2 and 3b–f). The cone and the platform were designed to match their axis with
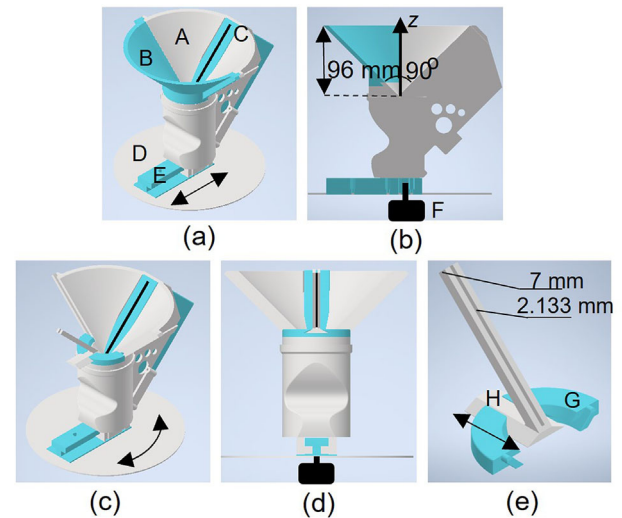

FIGURE 3 Conical container design overview. (a) Cone container with inserted half cone. A - the cone, B is the detachable half-cone. C – US transducer where the black line depicts the central line of the linear array. D – rotating platform. E – the rail. The arrows depict the directions in which the cone can be manually translated. (b) Lateral cross-section of the cone with inserted half-cone. F is a stepper motor, z is the spatial axis. (c) Cone with the half-cone replaced with the slit-holder and the slit. The arrows depict the platform can be rotated. (d) The slit is installed in front of the transducer array to guarantee the visibility of the needle in B-mode US images. (e) The biopsy slit inserted into the slit-holder. H – the biopsy slit. G – the slit holder. The arrows indicate the slit can be translated within the slit-holder.

the rotational axis of the motor (Figure 2). Therefore, no spatial calibration was needed. During the full revolution, the system acquires a set of 2D images (N >309), which further utilized for 3D reconstruction.[14] The cone should be filled with an acoustic coupling medium. In this work, we used a physiological saline solution (0.9% NaCl, 99.1% distilled water).

The cone has an opening angle of 90° and a height of 96 mm (Figure 3b) and can accommodate a prone-positioned breast of cup size A and B without any contact either with the wall of the cone or the transducer surface during the volumetric scanning. The transducer array (Figure 3a–c) was fixated in the cone and partially covered by cone material. As a result, 113 mm of the 152 mm length array could be used for imaging.

The cone is attached on the platform with a rail. The cone is inserted into a rail facilitating a linear translation of the cone towards the breast in the plane matching the US B-mode plane. The cone can be manually moved along the rail with minimal friction and fixed at any position with a lock.

To perform a breast biopsy, the coupling medium should be drained out of the cone through a hose. Subsequently, one half of the cone opposite to the transducer can be detached providing the interventionist a window for direct breast access. Meantime, the remaining half of the cone serves a breast support during the
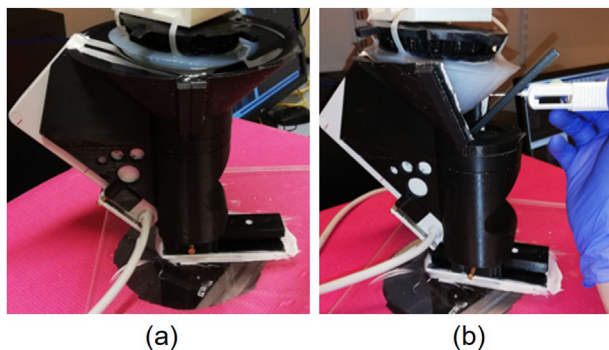
FIGURE 4 ACBUS-BS system in (a) 3D scanning and (b) biopsy modes.

biopsy procedure. To direct the needle during the biopsy procedure, we provide a needle slit that is attached to the cone as shown in Figure 3b and d. The slit is inserted by the operator in a designed holder in front of the US transducer and it keeps the needle within the US plane. The slit can be translated towards the breast for better positioning of the needle. Photos of the cone made during 3D image acquisition and biopsy are provided in Figure 4.

The ACBUS-BS is operated from a workstation (personal computer, Intel Xeon CPU (2 × 2.40 GHz), and 64 GB RAM) using a graphical user interface (GUI) custom developed in Matlab 2019b (MathWorks, Natick, US). The GUI allows the user to rotate the motor by activating trigger pulses on an Arduino Uno (Arduino LLC, Boston, USA) connected to the motor, gives B-mode image feedback to the user, and highlights the target on these B-mode images which enables targeting of US-occult lesions.

The data from the ABVS system are captured by the workstation PC via a frame grabber. The image acquisition is synchronized with the increment of the cone, excluding latency due to image transfer. Consequently, no temporal calibration was required.[19]

2.3 | Biopsy procedure overview

The biopsy procedure consists of four basic steps: target localization and segmentation, positioning, preparation, and biopsy. The first step, in which the position of the lesion to be biopsied is determined in the coordinate system of the cone, can be subdivided into sub-steps: pre-procedure MRI acquisition, 3D US acquisition, MRI-3D US image fusion, and target segmentation. A detailed description of the abovementioned steps and sub-steps is provided in the following sections. Notably, the two MRI-based sub-steps, that is, the abovementioned pre-procedure MRI acquisition and MRI – 3D US image registration can be omitted in case the lesion is not US occult.

2.4 | Target localization and segmentation

2.4.1 | Pre-procedure MRI acquisition

In the case of an US-occult lesion, the pre-procedure imaging step is aimed to acquire a reference volumetric image, where the biopsy target is clearly visible.

In our study, we used a 3 Tesla Skyra MRI (Siemens Healthcare, Erlangen, Germany) with T2 sequence and a Dixon protocol (fat series)[20] to acquire multi-slice 2D MRI data with voxel dimensions of 2.50 mm in transversal, and 0.94 mm in both the coronal and sagittal directions. During the MRI acquisition, the phantom was positioned within the RF coil such that the sagittal axis (Figure 1a) was directed to ground, mimicking the data acquisition from the patient in a prone position.[21] We made sure the phantom was as close to the isocenter as possible in order to avoid geometrical distortion.

2.4.2 | 3D US acquisition

For US-occult lesions the next sub step is to acquire volumetric ultrasound data using the ACBUS-BS device. For lesions visible on US this is the first step of the biopsy procedure. During the acquisition, the phantom was positioned in the cone such that the sagittal axis was directed to the ground mimicking the data acquisition from the patient in a prone position. The cone was filled with saline solution and 2D ultrasound data were acquired while the cone was making a full rotation around the phantom. The acquired B-mode images were stored on a local workstation PC, and used for volumetric image reconstruction, as described in.[14] The acquisition time was 90 s and the reconstruction time for the breast volume of 500 μm isotropic voxel size was 209 s.

2.4.3 | MRI-3D US image registration

The aim of this sub step which is required for US-occult lesions only, is to register the MRI data to the 3D US data.

Various non-rigid and rigid-based registration methods have been proposed for multimodality volumetric image fusion. In the current version of the ACBUS-BS, a rigid surface-based registration method utilizing an iterative closest point algorithm (ICP)[22] was used for MRI-3D US image registration. Our group has demonstrated in[14] that rigid transformation can also be applied for in vivo breast. Herein, for in vivo measurement, the MRI scanning of the volunteer was performed while the breast was positioned in a cone filled with the saline solution. It was demonstrated that the same shape was
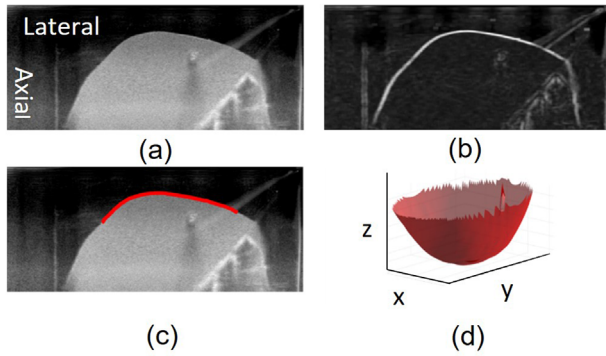
FIGURE 5 Surface segmentation algorithms steps. (a) Initial image. (b) Filtered image. (c) Extracted surface. (d) Rendered surface.

retained in both modalities leading to a registration error of only 2.23 mm with a single cyst used as a validation marker.

For automatic segmentation of the breast surface in the acquired 3D US data, a custom algorithm was utilized. A sliding window (10×10 pixels) was applied to each 2D image. Each pixel of the filtered image was assigned a value equal to the standard deviation of the values of the pixels within the sliding window for each iteration. The coordinates of the surface on the B-mode image were derived from the points with maximum standard deviation along each image line. The result of the segmentation is shown in Figure 5. The example of displayed targets after the localization step is shown in Figure 6a and b.

For the PVA phantom, we calculated a registration error (e_r) as the Root Mean Squared Error (RMSE) between the coordinates of centres of segmented visible lesions in 3D US data (observed positions) and centers of segmented corresponding lesions in MRI data after registration. Besides, we calculated average Dice coefficients with corresponding lesions' volumes. For the in vivo approximation, the registration error e_r was taken from[14] and was equal to 2.23 mm.

The vector of the registration error can point in to any direction of 3D space.

2.4.4 | Target segmentation

Lesions visible on US could be directly segmented manually in 3D US data acquired with the cone using the GUI.

For US-occult lesions, the target, as well as breast surface, were first segmented semi-automatically in pre-procedure MRI data using a region growing algorithm implemented in 3D Slicer 4.10.2 Software.[23] The segmented data were exported in STL format for importing into the operating software.

Importantly, inaccurate lesion segmentation, that is, segmentation error (e_s) can further lead to a wrongly

localized biopsy target. In this study, the segmentation error for the PVA phantom is neglected ($e_s = 0$), since the lesions are spherical and have high contrast with respect to the background in MRI due to the gadolinium. Although the spherical inclusions in MR data typically have an increased radius compared to US, this does not lead to segmentation errors since the spherical inclusions remain concentric.

Nevertheless, the perfect spherical shape for in vivo lesions is rare, and the segmentation error will affect the biopsy accuracy. Therefore, for the in vivo approximation, we use in vivo data acquired from a cyst which were published in.[14] Herein, e_s was equal to 0.64 mm and was calculated as the absolute difference between radiuses of lesions segmented in MRI (lesion's volume is 600 mm^3) and 3D US (lesion's volume is 405 mm^3) data.

The vector of the segmentation error can point in any direction of 3D space.

2.5 | Positioning

After the lesion has been localized in cone coordinates, the cone is rotated at the angle β such the US plane contains the geometrical center of the target and to minimize the biopsy path length. Once in this plane, the operator initiates recording of B-mode data using the GUI. The recording should last until the operator has prepared the breast for biopsy and should be switched off manually.

The rotation angle β is defined as the angle at which the cone should be rotated to align the needle with the lesion (see also Figure 6a). For a lesion located at L (L_x, L_y) this angle can be calculated following:

$$\beta = \begin{cases} \tan^{-1}(L_y/L_x), & L_x > 0, \\ \pi + \tan^{-1}(L_y/L_x), & L_x < 0, \\ \frac{\pi}{2} \cdot sign\left(L_y\right), & L_x = 0. \end{cases} \quad (2)$$

The number of discrete rotation angle steps N_β by which the motor is moved to approximate that angle follows from:

$$N_\beta = \left[\frac{\beta}{\Delta_\beta}\right], \quad (3)$$

where Δ_β is the rotation step size of the motor in radians.

Due to the discrete nature of the parameter N_β, the system can only be navigated at discrete points in space that can be slightly different from the actual location of the target. The navigation error (e_n) is anisotropic and can be calculated in x- and y-direction. The maximum navigation error occurs when the target lesion is
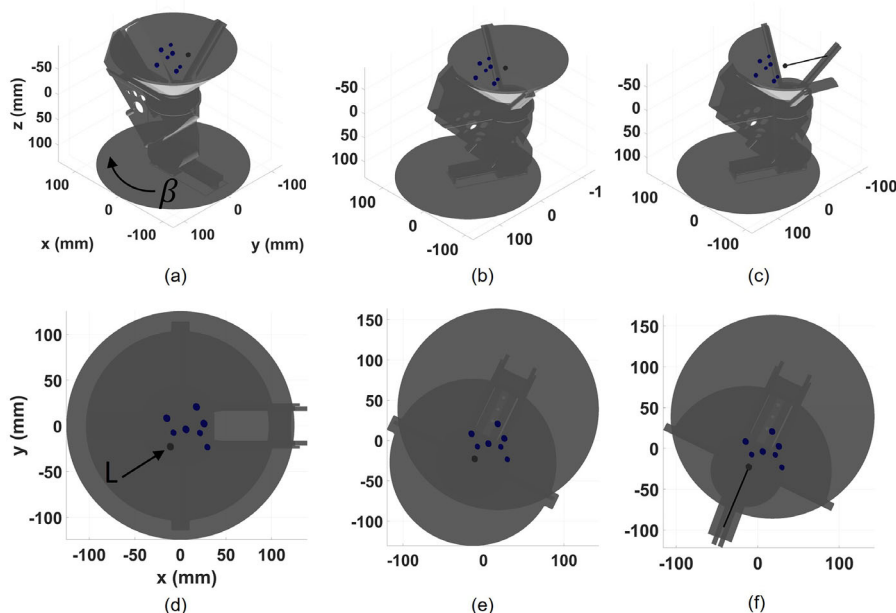
FIGURE 6 Biopsy procedure overview. (a, d) Initial position of the cone. In this image the localized target L is indicated with an arrow. (b, e) The cone is brought into position for taking a biopsy, i.e., rotated and translated against the breast. (c, f) The half-cone is replaced with the biopsy slit. The black line suggests the needle trajectory.

at equal distance from the two nearest available discrete navigation points and can be calculated using:

$$
\begin{cases}
e_n = \sqrt{e_{n,x}^2 + e_{n,y}^2}, \\
e_{n,x} = R_{cone}\left(1 - \cos\left(0.5\Delta_\beta\right)\right), \\
e_{n,y} = R_{cone}\sin\left(0.5\Delta_\beta\right),
\end{cases}
\tag{4}
$$

where e_n is the navigation error, $e_{n,x}$ and $e_{n,y}$ are the maximum navigation errors in x-, y- direction; R_{cone} is the radius of the cone's base.

The navigation e_n error is transversal to the US plane.

After the transducer is in the right imaging plane, the cone is translated towards the breast until it is in direct contact with the breast. In the current version, the translation is performed manually by the operator by moving the cone along the rail and using real-time B-mode images as visual feedback. An example of the positioning step is shown in Figure 6c,d.

Notably, the cone translation will result in breast deformation leading to the relocation of the target lesion. This issue is addressed in the following section.

2.6 | Preparation and biopsy

Next, to prepare the breast for biopsy, the operator drains the coupling medium from the cone through the tube attached to a sealed hole on the cone. The draining of the coupling medium will also induce breast deformation and target lesion relocation. This issue is addressed in the next section.

The removable half of the cone opposite to the US transducer is detached by the operator to gain direct access to the breast's surface. Then the operator should install the biopsy slit, see Figure 6c and f. Next, the operator can prepare the breast surface for biopsy by processing it with a disinfectant and making an incision. The recorded image data are used to update the position of the target lesion after the abovementioned manipulations. Afterward, based on the updated position of the target, the software calculates the insertion trajectory parallel to the chest wall. Additionally, the software indicates the height of the insertion point from the opening of the cone. Finally, the biopsy can be performed. The preparation time including the time spent for coupling medium (200 mL) draining is less than 90 s.

Similar to the MRI-guided biopsy, the physician is operating under the table while being seated on a chair[24] slightly beneath the level of the operating table. A 14-gauge needle was use for biopsy. An example of the positioning step is shown in Figure 6c and f.

To evaluate the biopsy performance, we calculated the average length of stained material for both US occult and US-visible lesions in the PVA phantom.

2.7 | Lesion relocation estimation

As expected, the cone's translation, coupling medium draining, and needle insertion may lead to a relocation of the target lesion from the initially determined position. Therefore, we track the target's center displacement from the initial state, that is, before transducer's

translation, to the new direct access state by using cross-correlation-based tissue motion estimation applied to the series of consequently acquired B-mode images.[25]

An initial circular region of interest (ROI) corresponding to the lesion was determined automatically in the target localization step. We assume the displacement of the ROI is equal to the displacement of the target lesion. The tracking was achieved using the abovementioned cross-correlation-based tissue motion estimation[26,27] with a template of 10×10 pixels and a search kernel of 20×20 pixels. The displacement was calculated for each pixel belonging to the ROI in lateral, and axial directions of the US transducer. Finally, the center of the ROI was translated on above-calculated values in corresponding directions, and a new ROI of the radius was defined in the new center. Those steps were repeated for each pair of consequently acquired frames.

To minimize the influence of randomly displaced pixels on the overall displacement estimation, first, the calculated lateral (along the transducer's surface) and axial (transversal to the transducers surface) displacements of each pixel within the ROI were combined into a complex number. Next, we calculated the mean direction of the displacement. Only the pixels which are co-directed to the mean translational direction with a deviation of 22.5° were considered for the final calculation of the displacement of the lesion's center. So, the discrete displacement can be calculated as described below:

$$\begin{cases} \Delta_l = \langle Re(z) \rangle, \\ \Delta_a = \langle Im(z) \rangle, \end{cases} \quad (5)$$

where z is a complex number comprising lateral and axial displacements as real and imaginary parts respectively for each pixel and $|\angle z - \angle \sum z| < 22.5^{\circ}$, Δ_l and Δ_a are discrete displacements of the center of ROI, i.e., target lesion, in lateral and axial directions respectively. Finally, the position of the ROI's center is shifted by these discrete displacements and then, redefined as the new center. The next discrete displacements are calculated based on the updated ROI.

We tested the performance of the algorithm on CIRS and PVA phantoms in three cases: cone translation, coupling medium draining, and needle insertion by calculating the tracking error (e_t). The error was measured as RMSE with respect to a manually segmented lesion's center. Before calculating the RMSE, both, observed and estimated trajectories, were smoothed with a median filter with kernel size of 10 samples. To characterize the system, for each phantom type we use an aggregated tracking error from 3 abovementioned cases assuming the errors are co-linear and co-directed.

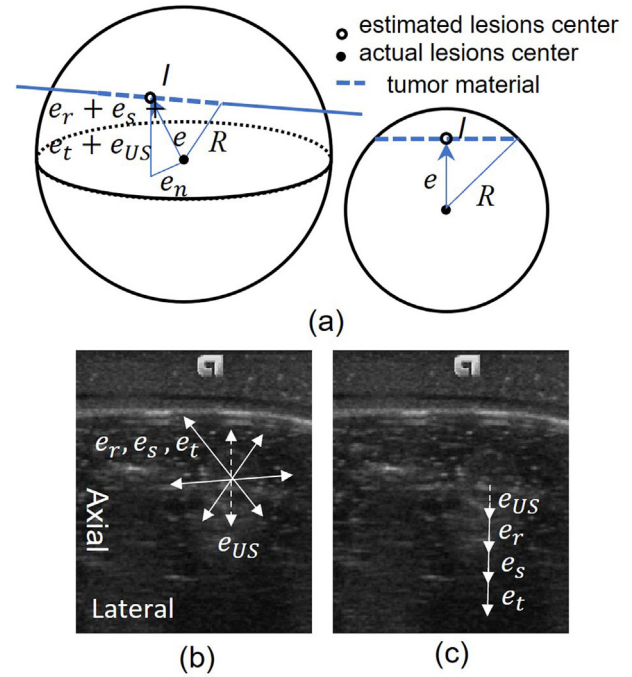The vector of the tracking error belongs to the US plane and can point in any direction.

FIGURE 7 Schematic of error's impact on the tumor material length and estimated lesion's position. (a) The impact of the total error on the tumor meterial length in the biopsy sample. (b) The direction of errors belonging to the US plane. The US accuracy error (dashed arrow) is parallel to the axial axis whilst the rest of errors are can point in any directions (solid arrows). (b) In the worst-case scenario, the segmentation and registration errors fully belong to the US plane. Furthermore, all errors are aligned in axial direction.
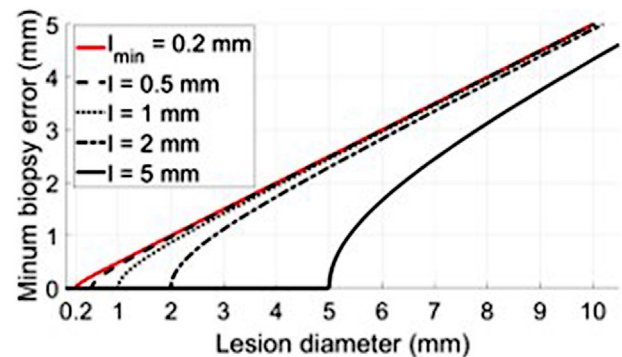

FIGURE 8 Minimum biopsy error as a function of lesion diameter for different tumor material lengths *l*.

In the current version of the software, the displacement is not calculated in real-time. However, the measured time needed to calculate one discrete displacement was ~2 s.

2.8 | US accuracy error

The inaccuracy of US (US inaccuracy error e_{US}) imaging is related to the presence of different tissue types with different sound speeds whilst a fixed sound speed

TABLE 1 Registration accuracy.

DSC	e_r (mm)	V_{MRI} (mm^3)	$V_{3D\ US}$ (mm^3)
0.69 ± 0.10	1.33 ± 0.66	231.00 ± 72.96	192.88

DSC, Dice - Sørensen Coefficient; d, distance between the geometrical centers of the lesions; V_{3DUS}, calculated lesions' volume within 3D US.

is considered for the US image reconstruction. The vector of the inaccuracy error is parallel to the axial axis of the US image and can be estimated with the equation below:

$$e_{US} = z_l \left| 1 - \frac{c_{US\ system}}{<c_{sample}>} \right|, \qquad (6)$$

where z_l is a distance between the lesion and the transducers surface, $c_{US\ system}$ is a speed of sound embedded in the US system for reconstruction, and $<c_{sample}>$ is an average speed of sound of the imaged object. The distance z_l is considered 10 mm as the US occult lesions do not lay deeper in the phantom that 10 mm. We also did the estimation of the US inaccuracy error for in vivo approximation for $z_l = 10$ mm. We used 1520 m/s as a speed of sound in a breast.[28]

2.9 | Biopsy accuracy

Successful biopsy implies the presence of sufficient tumor material length l_{min} for histopathological work-up

which is at least 0.2 mm.[29] The minimal length of tumor material that will be excised by ACBUS-BS for a lesion with a certain radius (considering it is spherical) given a certain biopsy error can be calculated with a formula below which is supported by Figure 7:

$$l = 2 \cdot \sqrt{R^2 - e^2}, \qquad (7)$$

where l is the tumor material length, R is the lesion's radius, e is the total biopsy error. The dependence of e on the lesion diameter for different l is depicted in Figure 8.

The e_n is perpendicular to US plane. The projections of e_s and e_r on the US plane can belong to any direction as well as e_t, whilst e_{us} is always parallel to the axial axis (Figure 7b). Therefore, the total error is maximized when e_s and e_r belong to US plane, e_s, e_r, e_{us}, and e_t co-linear and co-directed in axial direction (Figure 7c). Consequently, the total error can be calculated with the formula below:

$$e = \sqrt{e_n^2 + (e_r + e_s + e_t + e_{US})^2}. \qquad (8)$$

We calculated the tumor core length for the PVA phantom with estimated total error and given lesion's radius. Finally, for invivo approximation, we calculated the minimum lesion's diameter at which the presence of sufficient tumor material length for the histopathological work-up ($l = l_{min}$) is guaranteed.
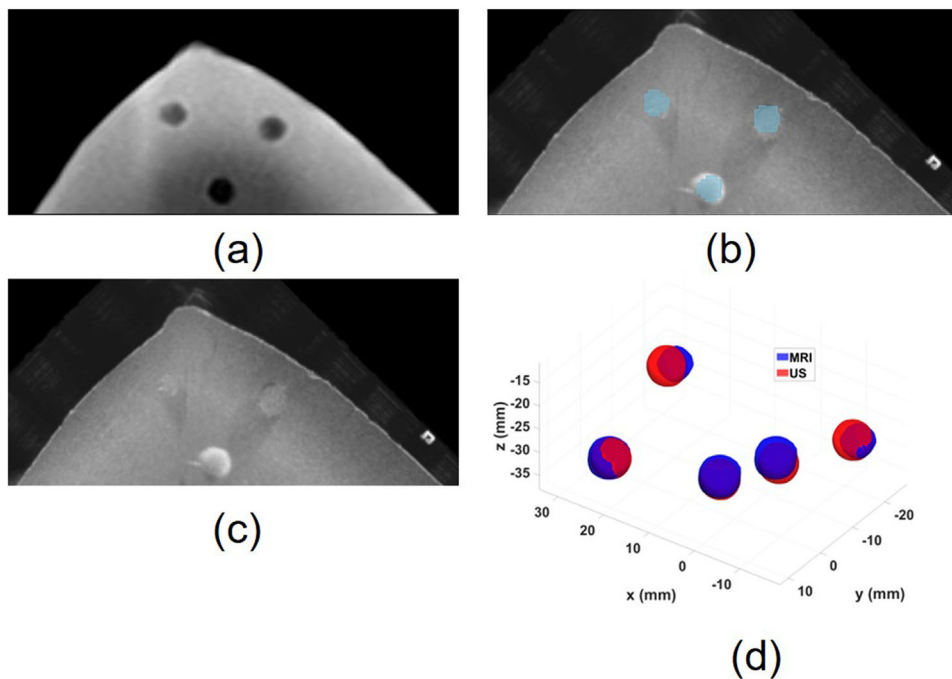

FIGURE 9 (a) MRI – (c) 3D US PVA phantom image registration. (b) The lesions, segmented in MRI are superimposed with 3D-US data. (d) The overlapped lesions from MRI and 3D US data.
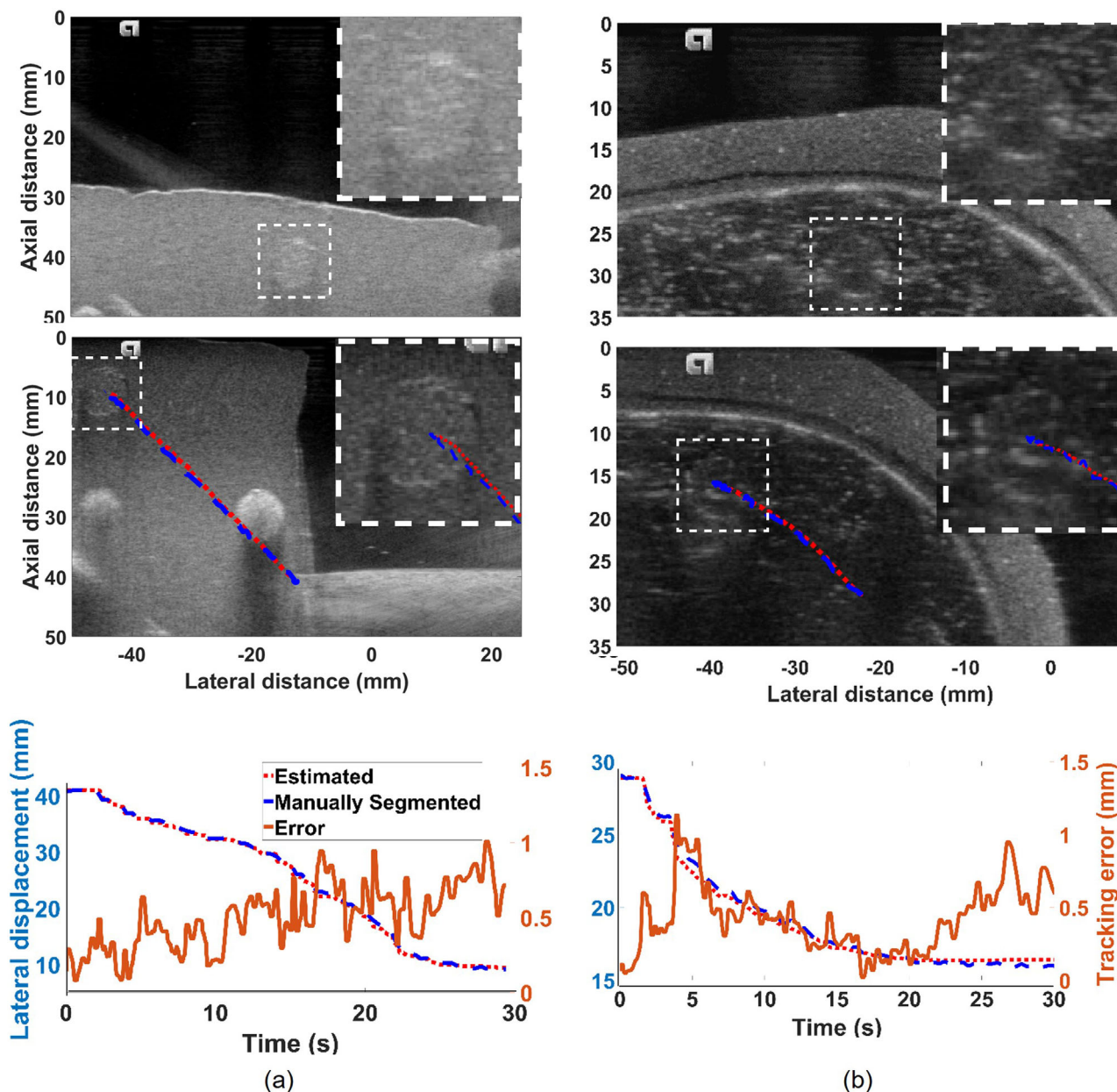
FIGURE 10 Displacement tracking during cone translation for (a) PVA and (b) CIRS phantom. Top row demonstrates the lesion position before the cone has been translated. Middle row demonstrates the lesions position after translation with manually segmented (blue) and estimated (red) trajectories. The bottom plots show the segmented and estimated trajectories of the lesion in lateral directions as well as difference between them.

3 | RESULTS

3.1 | Phantom characterization

The median stiffnesses for the homogeneous PVA and CIRS phantom were measured to be 7.6 and 28 kPa, respectively.

For the PVA phantom, CNRs for high and low contrast inclusions are 14.67 ± 0.95 and 3.39 ± 3.15 dB, respectively. The CNR for the inclusions in CIRS phantom was calculated as -6.63 ± 3.81 dB. The speed of sound within the PVA was calculated as 1460 m/s.

3.2 | Registration

The registration metrics are presented in Table 1. Images highlighting the results of the MRI-3D US image fusion are presented in Figure 9. In the center panel, the MR-based segmentation is presented as an overlay on
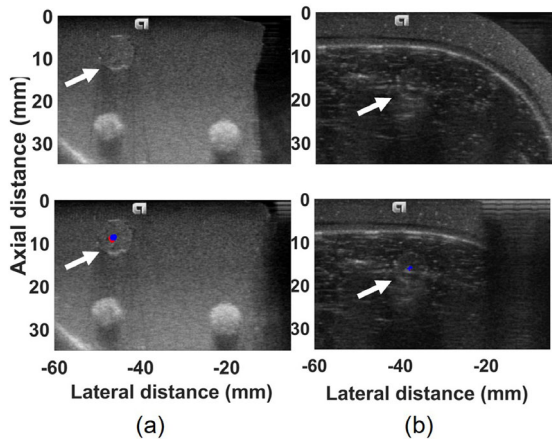
FIGURE 11 Displacement tracking during coupling medium draining for (a) PVA phantom and (b) CIRS phantom. The white arrow points at the tracked lesion. The tracked lesions are indicated with white arrows.
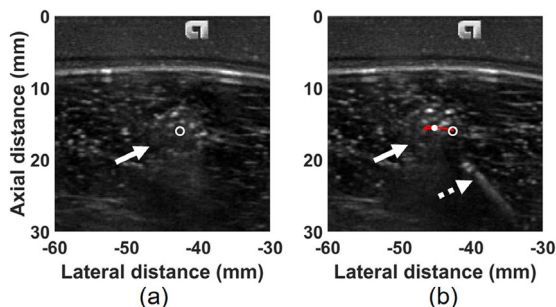

FIGURE 12 Displacement induced by the needle insertion into the CIRS phantom. (a) Before insertion. (b) After insertion. The lesions trajectory is depicted with a red line. The initial position of the lesion is depicted with the hollow circle while the end position of the lesion is depicted with the solid circle. The tracked lesion is indicated with a white arrow. The biopsy needle tip is indicated by the dashed line.

TABLE 2 Tracking error estimation.

Phantom's name	e_t (mm) for three cases		
	Cone's translation	Coupling medium draining	Needle insertion
PVA	1.06 ± 0.52	0.55 ± 0.20	0.51 ± 0.30
CIRS	0.42 ± 0.24	0.37 ± 0.17	0.31 ± 0.12

the 3D-US data. The measured time required for fusion was less than 10 s.

3.3 | Lesion relocation estimation

The cumulative tracking errors for PVA and CIRS phantoms are 2.12 and 1.10 mm, respectively.

The displacements induced by translation of the cone, draining of the coupling medium, and needle insertion

are depicted in Figures 10 to 12. The highlighted target is not depicted on those figures for demonstration purpose.

The maximum displacement due to needle intervention into PVA and CIRS phantom were 1.90 and 4.08 mm, respectively. The measured tracking errors for both, PVA, and CIRS phantoms are presented in Table 2. The displacement of the lesion embedded in the CIRS phantom is presented in Figure 10. The time spent for coupling medium draining (200 mL) from the current version of the cone was 23 s. The rest of the preparation steps take less than 1 min.

3.4 | US accuracy

The US accuracy for the PVA phantom and in vivo approximation were 0.55 and 0.13 mm, respectively.

3.5 | Biopsy

All eight biopsies were performed under real-time ultrasound guidance as shown in Figure 13. The eight biopsied samples are presented in Figure 14. The average size of the stained material within the biopsy samples was 7.00 ± 0.92 mm and comprises 6.33 ± 1.16 mm for US occult lesion and 7.40 ± 0.55 mm for non-US occult lesions. The needle was visible in US during all biopsies.

3.6 | System limitation

The calculated errors for the PVA phantom and in-vivo approximation are summarized in Table 3. For the PVA phantom with spherical lesions of 10 mm in diameter, the minimal length of tumor material to expect within the sample was determined to be 5.97 mm, according to Equation (7).

For in vivo approximation with a total biopsy error of 4.11 mm, the ACBUS-BS can deliver sufficient length of the tumor material, that is, 0.2 mm, for lesions larger than 8.22 mm in diameter.

4 | DISCUSSION

In this paper, we introduce and evaluate a novel device for combining volumetric ultrasound imaging and biopsy guidance, the ACBUS-BS. This device was successfully used to perform biopsies in a custom-developed soft breast-shaped phantom containing stained inclusions mimicking lesions, where part of the inclusions was US occult. The ACBUS-BS enables the navigation on US-occult lesions by utilizing 3D US – MRI image fusion and lesion displacement tracking. Therefore, the system facilitates easy targeting of the lesions reducing the need for MRI-guided biopsy.
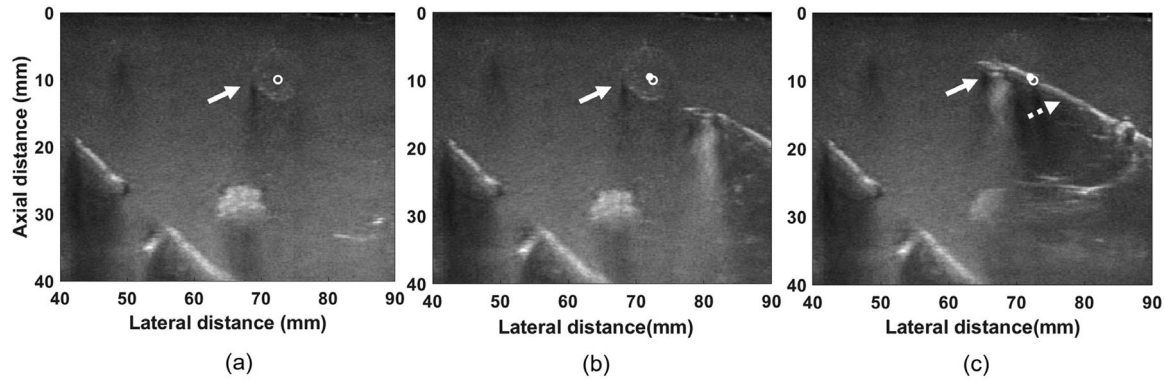
FIGURE 13 B-mode US images during the biopsy US-occult lesion. (a) Before the needle insertion. (b) Before the needle aspiration. (c) During the aspiration. The dashed arrow points at the needle. The solid white arrow points at the US-occult lesion. The hollow circle indicates the localized center of the lesion after the coupling medium draining. The solid circle indicates the localized center of the lesion after the needle insertion.
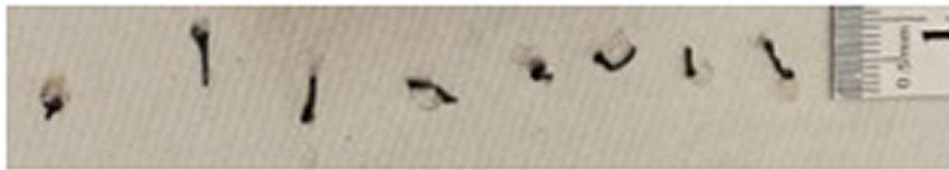

FIGURE 14 Biopsy results.

Besides, the ACBUS-BS system was designed to facilitate a biopsy procedure under sterile conditions. The interventionist has a direct access to the breast surface enabling processing and preparing the breast surface alike for a conventional US-guided biopsy.

Finally, the ACBUS-BS can facilitate biopsy of the lesion, located close to the chest wall. It was also demonstrated[14] that scanning with the cone also facilitates imaging of the area near the chest-wall with sufficient penetration of the US transducer.

Figure 14 confirms successful biopsy of all lesions by presence of stained material within each sample. The average biopsy tumor core size was 7.00 ± 0.92 mm, which is 17% higher than the predicted value of 5.97 mm. The result demonstrates that the total error is less than the theoretically derived worst-case total error which was calculated based on the assumption that all errors (except the navigation error) are occurring only within the US plane, are co-linear and co-directed (Figure 7). Also, in vivo we expect this worst-case scenario not to occur, and thus, the total error due to the mentioned error sources to be smaller. However, if we do consider the worst-case scenario the presence of a biopsy sample sufficient for histopathological work up is guaranteed for lesions larger than 8.22 mm in diameter (Table 3, Figure 8).

It should be noted that for non-spherical lesions and small lesions the total error calculation is not valid. For instance, if the lesion size is less than the sum of the segmentation and the registration errors and the errors

TABLE 3 Biopsy error.

	e_r (mm)	e_t (mm)	e_n (mm)	e_s (mm)	e_{US} (mm)	e (mm)
PVA phantom	1.33	2.12	0.30	0	0.55	4.01
In vivo approximation	2.23	1.10	0.30	0.64	0.13	4.11

are perpendicular to the US plane, the target will not even intersect with the US plane leading to a failed biopsy.

We will now first discuss how the error of the entire procedure can be further reduced. After that we will discuss other potential sources of error, followed by a discussion on limitations and possible future improvements of the device, and conclude with a discussion on the clinical merit of the device.

The total biopsy error can be mostly diminished by reducing the registration error, which is dominant for the in vivo case. This might be possible by a marker-based registration: internal anatomical landmarks, for example, visible lesions, and external markers. For instance, multimodality MRI - US breast silica markers[30] might be a good candidate for this application.

Another way to reduce the total error is by reducing the error due to navigation, which is mainly a consequence of the discrete nature of navigation. Thus, the error can be reduced by using a stepper motor with a smaller discrete step-size.

One source of error which was neglected in the current study and might come into play in vivo is geometrical distortion when tissue is further away from the MR isocentre.[31,32]

Another potential source of error when applying ACBUS-BS in vivo relates to the fact that the toughness of real tissue is much higher than that of the phantoms used and therefore would possibly create greater amounts of tissue deflection during the needle insertion. However, we do not expect any additional impact of this factor on the biopsy procedure for the following reasons. First, in the ACBUS-BS the breast is supported by the half-cone on the opposite to the needle insertion side, which limits breast deflection and prevents large displacement due to needle intervention (Figure 4). The designed biopsy slit enables the interventionist to maneuver with the needle within the US imaging plane. Second, real breast tissue has inhomogeneous echogenicity and a more diverse speckle pattern which will improve the accuracy of displacement estimation/lesion tracking. For instance, during needle insertion, the maximum lesion displacements measured were 1.90 and 4.08 mm for PVA and CIRS phantoms, respectively, while the displacement errors were 0.31 ± 0.12 and 0.51 ± 30 mm for CIRS and PVA phantoms, respectively (Table 2).

It should be noted that with the current setup the speckle tracking can only compensate for in-plane lesion relocation induced by positioning and preparation of the container to the biopsy, since during those steps only series of consequently acquired 2D images are available with the currently used linear array probe. Hence, no compensation for out-of-plane motion was possible yet and this motion was considered negligible. Replacing the linear array probe by a dedicated matrix array and extending the speckle tracking software from 2D to 3D would enable compensating for potential out-of-plane motion in future.

Another potential source of error which will have to be considered before the ACBUS-BS is used on patients, is the error induced by patient motion. The motion can occur during either 3D US acquisition, or biopsy. The motion due to respiration is not taken into consideration since patient is in a prone position during all acquisitions.[33] Patient motion occurring during 3D US acquisition can be minimized by ensuring the patient is in comfortable position. Furthermore, the patient should be instructed not to move during the entire procedure. In future versions of the system, we are also considering to use plane wave transmission-based ultrasound scanning, which is at least 10 times faster as demonstrated by Hollander et al.[34] Since reduced acquisition time reduces the chance of motion occurrence, this will also reduce the impact of patient motion. Patient motion occurring during biopsy can be compensated for by speckle tracking, although this will require a real-time performance of the algorithm.

In our study we only used a 14 G needle and our slits exactly matched the outer needle diameter. By making sure the needle tidily fitted the biopsy slit we ensured the needle was kept within the US image plane. The needle was visible during all biopsies. Nevertheless, it should be noted that when the slit is even 0.5 mm wider than the outer diameter of the needle, it can create error of more than 10 at 50 mm distance from the slit. Finally, in clinical practice biopsies can be taken with needles of various sizes, that is, 14, 15, 16, or 18-Gauge.[35] When using other needles, also dedicated slits will need to be developed.

The segmentation and registration errors might also be perpendicular to the US plane. In case the sum of those error exceeds the radius of the lesion, the target will not even intersect with the US plane leading to the failed biopsy. The out-of-plane error can mostly be reduced by utilizing a more accurate registration method.

In this work, we used rigid surface-based registration that can deliver the registration accuracy of 2.23 mm.[14] Various non-rigid and rigid-based registration methods have been proposed for multimodality volumetric image fusion. Tagliabue et al. compared performance of a finite element (FE) method and a novel position-based dynamics method (PBM) to model a displacement after applying an external force to the abovementioned CIRS breast phantom. The reported registration errors were 4.32 ± 1.82 mm for the FE method and 3.89 ± 1.50 mm for the PBM method.[36] Alternatively, Han et al. applied a combination of affine, FE, and free-form deformation (FFD) to simulate a shape transformation of a real breast induced by repositioning it from prone to supine position. The reported average error was 4.4 mm with a maximum error of 7.6 mm.[37] So, to our knowledge, the registration method utilized in this work can deliver better registration accuracy compared to the non-rigid registration methods developed for breasts.

The rigid surface-based registration requires the breast to be immersed in water during the MRI scanning.[14] Admittedly, it is impractical to modify the MRI screening routine by introducing a water bucket in the MRI scanner. Nevertheless, in the proposed scanning method the breast immersed in the cone is deformed with known boundary conditions, that is, buoyance forces acting around the breast surface. Thus, it should be feasible to develop a novel application-specific deformable model based on the abovementioned assumptions in the future.

The current version of the ACBUS-BS is not yet applicable to breast with a cup size larger than B due to the fact that the clinical scanning presets of the S2000 system limits the penetration depth of the transducer to ~60 mm. Thus, the current version of ACBUS-BS utilizes only ~65% of the total transducer's length. By increasing the penetration depth, it is possible to incorporate the full 152 mm width of the 14L5BV transducer

which will enable increase of the cone's volume. The penetration depth can be increased by using ultra-fast ultrasound scanning as demonstrated by Holländer et al.[34] Besides, we recently demonstrated for a hand-held 14L5 transducer, which has the same specs as the 14L5BV transducer, that coherent compounding of ultra-fast transmit the penetration depth by 20 mm without decreasing resolution. Adaptation of the cone for the breast of cup size D without additional scanning time has already been discussed in.[14]

In the current implementation of the ACBUS-BS operating software, the displacement can only be calculated offline. However, as a further improvement, the algorithm will implement in high-level programming languages, such as C++ to reach real-time performance.

Currently, the biopsy process is semi-automatic. The lesion location is tracked by the speckle tracking algorithm. As a result, the interventionist can observe on the screen an updated center of the lesion to be biopsied. Based on the observed position of the target center the needle trajectory can be adjusted manually while the needle is kept within the US plane by the biopsy slit.

Nevertheless, the needle can be adjusted automatically. For instance, an automated needle guide end-effector[38] can be utilized to keep the biopsy needle within the US plane and automatically update the needle position based on the detected relocation of the biopsy target.

Additionally, the usability of the ACBUS-BS can be improved by automating the cone's translation. The last can be implemented by substituting the rail by a motor-actuated linear translation stage.

Volumetric ultrasound data of the breast can also be recorded by a technology called ultrasound tomography (UST). Besides recording echo signals in receive, UST also records through transmission ultrasound signals which enables quantifying the speed of sound and attenuation of breast tissue.[39] This modality can provide images with sensitivity and specificity comparable to MRI at less expense.[40] However, tomography does not provide real-time imaging feedback and is challenging to use for image guidance. Nevertheless, the combination of UST with ACBUS-BS can be a cost-effective tool for breast diagnosis. This combination excludes MRI from examination that is beneficial for patients with claustrophobia, metal implants or other contraindications for MRI.[5]

The ACBUS-BS setup has several advantages. Automatization of the biopsy navigation can save time for a radiologist as well as for the patient. The steps like lesion detection, biopsy planning, and needle placement can be omitted. Additionally, unlike MRI-guided biopsy or the approach demonstrated in,[13] the ACBUS-BS procedure does not require breast fixation, increasing patient's comfort. Thus, MRI scanning, and US biopsy can be performed in separate rooms enabling flexible scheduling and improved patient comfort. Furthermore,

ACBUS-BS also facilitates biopsy of lesions occult in US without requiring MRI-guided biopsy. Unlike MRI-guided biopsy, the ACBUS-BS does-not require large biopsy needles and can be performed in real-time.

Finally, we demonstrated the feasibility of the approach in a phantom. In vivo studies should follow to confirm its performance in patients.

5 | CONCLUSION

In this study, we presented a novel Automated Cone-based Breast Ultrasound Scanning and Biopsy System (ACBUS-BS). The system facilitates US-guided biopsy of lesions detected in pre-MRI and therefore might offer a low-cost alternative to MRI-guided biopsy. We demonstrated the feasibility of the approach by successfully taking biopsies of eight lesions embedded in a soft breast-shaped phantom, where three of them were US occult.

CONFLICT OF INTEREST

The authors declare no conflict of interest.

REFERENCES

1. Ferlay J, Steliarova-Foucher E, Lortet-Tieulent J, et al. Cancer incidence and mortality patterns in Europe: Estimates for 40 countries and 25 major cancers in 2018. *Eur J Cancer*. 2018;103:356–387. https://doi.org/10.1016/j.ejca.2018.07.005
2. Richardson LC, Royalty J, Howe W, Helsel W, Kammerer W, Benard VB. Timeliness of breast cancer diagnosis and initiation of treatment in the National Breast and Cervical Cancer Early Detection Program, 1996–2005. *Am J Public Health*. 2010;100(9):1769–76. https://doi.org/10.2105/ajph.2009.160184
3. Del Cura JL, Coronado G, Zabala R, Korta I, López I. Accuracy and effectiveness of ultrasound-guided core-needle biopsy in the diagnosis of focal lesions in the salivary glands. *Eur Radiol*. 2018;28(7):2934–2941. https://doi.org/10.1007/s00330-017-5295-9
4. Sood R, Rositch AF, Shakoor D, et al. Ultrasound for breast cancer detection globally: a systematic review and meta-analysis. *J Glob Oncol*. 2019;5:1–17. https://doi.org/10.1200/jgo.19.00127
5. Mann RM, Balleyguier C, Baltzer PA, et al. Breast MRI: EUSOBI recommendations for women's information. *Eur Radiol*. 2015;25(12):3669–78. https://doi.org/10.1007/s00330-015-3807-z
6. Schueller G, Schueller-Weidekamm C, Helbich TH. Accuracy of ultrasound-guided, large-core needle breast biopsy. *Eur Radiol*. 2008;18(9):1761–73. https://doi.org/10.1007/s00330-008-0955-4
7. Apesteguía L, Pina LJ. Ultrasound-guided core-needle biopsy of breast lesions. *Insights Imaging*. 2011;2(4):493–500. https://doi.org/10.1007/s13244-011-0090-7
8. Boba M, Kołtun U, Bobek-Billewicz B, Chmielik E, Eksner B, Olejnik T. False-negative results of breast core needle biopsies - retrospective analysis of 988 biopsies. *Pol J Radiol*. 2011;76(1):25–9.

9. Shah VI, Raju U, Chitale D, Deshpande V, Gregory N, Strand V. False-negative core needle biopsies of the breast: an analysis of clinical, radiologic, and pathologic findings in 27 conceccutive cases of missed breast cancer. *Cancer*. 2003;97(8):1824–31. https://doi.org/10.1002/cncr.11278

10. Youk JH, Kim EK, Kim MJ, Lee JY, Oh KK. Missed breast cancers at US-guided core needle biopsy: how to reduce them. *Radiographics*. 2007;27(1):79–94. https://doi.org/10.1148/rg.271065029

11. Dillon MF, Hill AD, Quinn CM, O'Doherty A, McDermott EW, O'Higgins N. The accuracy of ultrasound, stereotactic, and clinical core biopsies in the diagnosis of breast cancer, with an analysis of false-negative cases. *Ann Surg*. 2005;242(5):701–7. https://doi.org/10.1097/01.sla.0000186186.05971.e0

12. Imschweiler T, Haueisen H, Kampmann G, et al. MRI-guided vacuum-assisted breast biopsy: comparison with stereotactically guided and ultrasound-guided techniques. *Eur Radiol*. 2014;24(1):128–35. https://doi.org/10.1007/s00330-013-2989-5

13. Piron CA, Causer P, Jong R, Shumak R, Plewes DB. A hybrid breast biopsy system combining ultrasound and MRI. *IEEE Trans Med Imaging*. 2003;22(9):1100–10. https://doi.org/10.1109/tmi.2003.816951

14. Nikolaev AV, de Jong L, Weijers G, et al. Quantitative evaluation of an automated cone-based breast ultrasound scanner for MRI-3D US image fusion. *IEEE Trans Med Imaging*. 2021;40(4):1229–1239. https://doi.org/10.1109/tmi.2021.3050525

15. Gefen A, Dilmoney B. Mechanics of the normal woman's breast. *Technol Health Care*. 2007;15(4):259–71.

16. Gokhale S. Ultrasound characterization of breast masses. *Indian J Radiol Imaging*. 2009;19(3):242–7. https://doi.org/10.4103/0971-3026.54878

17. Surry KJ, Austin HJ, Fenster A, Peters TM. Poly(vinyl alcohol) cryogel phantoms for use in ultrasound and MR imaging. *Phys Med Biol*. 2004;49(24):5529–46. https://doi.org/10.1088/0031-9155/49/24/009

18. van Wijk MC, Thijssen JM. Performance testing of medical ultrasound equipment: fundamental vs. harmonic mode. *Ultrasonics*. 2002;40(1–8):585–91. https://doi.org/10.1016/s0041-624x(02)00177-4

19. Mozaffari MH, Lee WS. Freehand 3-D ultrasound imaging: a systematic review. *Ultrasound Med Biol*. 2017;43(10):2099–2124. https://doi.org/10.1016/j.ultrasmedbio.2017.06.009

20. Ma J. Dixon techniques for water and fat imaging. *J Magn Reson Imaging*. 2008;28(3):543–58. https://doi.org/10.1002/jmri.21492

21. Mann RM, Cho N, Moy L. Breast MRI: state of the art. *Radiology*. 2019;292(3):520–536. https://doi.org/10.1148/radiol.2019182947

22. Besl PJ, McKay ND. A method for registration of 3-D shapes. *IEEE Trans Pattern Anal Machine Intell*. 1992;14(2):239–256. https://doi.org/10.1109/34.121791

23. Fedorov A, Beichel R, Kalpathy-Cramer J, et al. 3D Slicer as an image computing platform for the Quantitative Imaging Network. *Magn Reson Imaging*. 2012;30(9):1323–41. https://doi.org/10.1016/j.mri.2012.05.001

24. Mann RM, Kuhl CK, Kinkel K, Boetes C. Breast MRI: guidelines from the European Society of Breast Imaging. *Eur Radiol*. 2008;18(7):1307–18. https://doi.org/10.1007/s00330-008-0863-7

25. Hendriks GAGM, Chen C, Hansen HHG, de Korte CL. 3-D single breath-hold shear strain estimation for improved breast lesion detection and classification in automated volumetric ultrasound scanners. *IEEE Trans Ultrason Ferroelectr Freq Control*. 2018;65(9):1590–1599. https://doi.org/10.1109/TUFFC.2018.2849687

26. Lopata RG, Hansen HH, Nillesen MM, Thijssen JM, De Korte CL. Comparison of one-dimensional and two-dimensional least-squares strain estimators for phased array displacement data. *Ultrason Imaging*. 2009;31(1):1–16. https://doi.org/10.1177/016173460903100101

27. Lopata RG, Nillesen MM, Hansen HH, Gerrits IH, Thijssen JM, de Korte CL. Performance evaluation of methods for two-dimensional displacement and strain estimation using ultrasound radio frequency data. *Ultrasound Med Biol*. 2009;35(5):796–812. https://doi.org/10.1016/j.ultrasmedbio.2008.11.002

28. Duck FA. *Physical Properties of Tissue*. London: Academic Press; 1990.

29. Edwards HD, Oakley F, Koyama T, Hameed O. The impact of tumor size in breast needle biopsy material on final pathologic size and tumor stage: a detailed analysis of 222 consecutive cases. *Am J Surg Pathol*. 2013;37(5):739–44. https://doi.org/10.1097/PAS.0b013e31828c63d0

30. de Jong L, Welleweerd MK, van Zelst JCM, et al. Production and clinical evaluation of breast lesion skin markers for automated three-dimensional ultrasonography of the breast: a pilot study. *Eur Radiol*. 2020;30(6):3356–3362. https://doi.org/10.1007/s00330-020-06695-y

31. Bagherimofidi SM, Yang CC, Rey-Dios R, Kanakamedala MR, Fatemi A. Evaluating the accuracy of geometrical distortion correction of magnetic resonance images for use in intracranial brain tumor radiotherapy. *Rep Pract Oncol Radiother*. 2019;24(6):606–613. https://doi.org/10.1016/j.rpor.2019.09.011

32. Nousiainen K, Mäkelä T. Measuring geometric accuracy in magnetic resonance imaging with 3D-printed phantom and nonrigid image registration. *Magma*. 2020;33(3):401–410. https://doi.org/10.1007/s10334-019-00788-6

33. Harvey JA, Hendrick RE, Coll JM, Nicholson BT, Burkholder BT, Cohen MA. Breast MR imaging artifacts: how to recognize and fix them. *Radiographics*. 2007;27(1):S131-45. https://doi.org/10.1148/rg.27si075514

34. Holländer B, Hendriks GA, Mann RM, Hansen HH, de Korte CL. Plane-wave compounding in automated breast volume scanning: a phantom-based study. *Ultrasound Med Biol*. 2016;42(10):2493–503. https://doi.org/10.1016/j.ultrasmedbio.2016.05.017

35. Helbich TH, Rudas M, Haitel A, et al. Evaluation of needle size for breast biopsy: comparison of 14-, 16-, and 18-gauge biopsy needles. *AJR Am J Roentgenol*. 1998;171(1):59–63. https://doi.org/10.2214/ajr.171.1.9648764

36. Tagliabue E, Dall'Alba D, Magnabosco E, Tenga C, Peterlik I, Fiorini P. Position-based modeling of lesion displacement in ultrasound-guided breast biopsy. *Int J Comput Assist Radiol Surg*. 2019;14(8):1329–1339. https://doi.org/10.1007/s11548-019-01997-z

37. Han L, Hipwell JH, Eiben B, et al. A nonlinear biomechanical model based registration method for aligning prone and supine MR breast images. *IEEE Trans Med Imaging*. 2014;33(3):682–94. https://doi.org/10.1109/tmi.2013.2294539

38. Welleweerd MK, Siepel FJ, Groenhuis V, Veltman J, Stramigioli S. Design of an end-effector for robot-assisted ultrasound-guided breast biopsies. *Int J Comput Assist Radiol Surg*. 2020;15(4):681–690. https://doi.org/10.1007/s11548-020-02122-1

39. Schreiman JS, Gisvold JJ, Greenleaf JF, Bahn RC. Ultrasound transmission computed tomography of the breast. *Radiology*. 1984;150(2):523–30. https://doi.org/10.1148/radiology.150.2.6691113

40. Duric N, Littrup P. Breast ultrasound tomography. *IntechOpen*. 2017, https://doi.org/10.5772/intechopen.69794